Nonlinear Dyn
https://doi.org/10.1007/s11071-022-07919-0

ORIGINAL PAPER

Nonlinear dynamics analysis in pneumatic tire modeling

Shunchang Duan · Xianxu Frank Bai · Qin Shi · Zhihao Liu

Received: 6 January 2022 / Accepted: 19 September 2022

Abstract Tires are the only link between vehicles and roads and provide all forces for vehicle movement, including driving, steering, and braking. Therefore, the tire model is fundamental for vehicle dynamics, and an efficient tire model is necessary for further technology development of vehicle dynamics and control. In this article, a simplified physical tire model featuring tire hysteresis properties is presented. Firstly, an elastic hysteresis system is introduced to the tire physical model. Then, combining with resistor–capacitor operator, force–deformation characteristics of the elastic hysteresis system are established. Correspondingly, the force–deformation characteristics are applied to describe tire nonlinear dynamics, and a unified expression of HysTire, i.e., a semi-empirical tire model featuring hysteresis characteristics, is established. Finally, the nonlinear dynamics of two tires are modeled to verify the effectiveness and superiority of HysTire. Comparison results with the magic formula model (MF) show that the HysTire provides accuracy like that of the MF, while it is much better in the profiles of predictive and extrapolative capabilities.

Keywords Semi-empirical tire model · Hysteresis · Pure braking or cornering condition · Vehicle dynamics · RC operator

S. Duan · X. F. Bai · Q. Shi
Engineering Research Centre for Intelligent Transportation and Cooperative Vehicle-Infrastructure of Anhui Province, Hefei University of Technology, Hefei 230009, People's Republic of China
e-mail: duan@mail.hfut.edu.cn

Q. Shi
e-mail: shiqin@hfut.edu.cn

S. Duan · X. F. Bai (✉)
Laboratory for Adaptive Structures and Intelligent Systems (LASIS), Department of Vehicle Engineering, Hefei University of Technology, Hefei 230009, People's Republic of China
e-mail: bai@hfut.edu.cn
URL: http://www.lasiser.com

Z. Liu
Xi'an Research Institute of High Technology, Xi'an 710025, People's Republic of China
e-mail: liuzh_epgc@163.com

1 Introduction

With the rapid development of electronics, control, and testing technology, advanced chassis control systems are constantly being developed to improve vehicles' safety, power, and comfort. Tires are the only parts that connect vehicles and roads. Except for the air force, controls of the vehicle's motion, including braking, acceleration, and steering, are achieved through the interaction between tires and ground. Efficient tire models are the foundation for accurate control of vehicle chassis [1]. However,

Published online: 03 October 2022

because the tire structure, material properties, driving environment, and working conditions are complex, the tire becomes an inherent nonlinear dynamic system with a complex coupling of lateral, longitudinal, and vertical responses. This is also the reason why tire nonlinear dynamics are difficult to describe.

Over the past half-century, scholars from different countries have proposed many tire models with different functions from different perspectives. In general, it can be divided into three categories according to the different modeling methods: theoretical, empirical, and semi-empirical models [2]. The theoretical tire model, also known as the analytical model or physical model, is used to simplify the tire's real physical structure, analyze the deformation mechanism in tire imprint, and establish a mathematical description of the tire nonlinear dynamics. Although the theoretical tire model cannot meet the requirements of calculation accuracy, it plays an important role in the qualitative explanation of the generation and action mechanism of tire's force and torque. In the classic brush tire model, tire body, belt layer, and actual crown element are replaced by an elastic brush element [3]. The tire body in the brush model is changed to an infinitely long elastic beam in Fiala model to study the tire cornering properties [4]. SWIFT model takes the tire body as a rigid ring and introduces an elastic element to represent residual stiffness, and the brush model is still adopted for the crown [5]. In FTire model, the tire belt layer is replaced by a certain number of band nodes and corresponding band segments to simulate the tire body, and an appropriate number of massless contact elements are inserted between adjacent band nodes to obtain the pressure distribution in the contact area [6]. The empirical model describes tire nonlinear dynamics directly by fitting test data under different working conditions. Therefore, the empirical model is consistent with test results and is convenient for applications. Currently, the most popular empirical model in the world is the Magic Formula model (MF) [6]. The MF is a set of combined trigonometric function formulas used to fit tire six-component force. The model formulas are ingenious and excellent in terms of the expressive power of tire nonlinear dynamics under various working conditions. Although the MF has quite ingenious and variable expression functions, it is poor in terms of the predictive power of untested properties, and much test data must be collected to obtain a practicable result [7]. The semi-empirical model combines advantages of the former two types of models, which not only achieves a high degree of theoretical accuracy, is good in terms of extrapolated power, and is clear in some basic physical and structural properties but also has a high degree of simulation accuracy and great consistency with test data. The UniTire model established by Guo is a semi-empirical formula of nonlinear dynamics under pure and combined working conditions, namely exponential formula, which is based on the Fiala model and guided by test data [8]. After nearly 30 years of development, the UniTire model has gradually developed and matured. It has a good expression ability for various working conditions and a simple model with outstanding prediction and extrapolation ability [9].

The nonlinear dynamics of tires are closely related to materials and structures. A tire is mainly composed of rubber, which is marked as a viscoelastic material [10]. Under certain conditions, viscoelastic materials possess the deformation properties of elastic and viscous substances in different mechanisms, which are the synthesis of elastic solids and viscous fluids, marked as viscoelasticity [11]. The materials viscoelastic theory mainly focuses on the material stress–strain relationship that is closely related to time, temperature, strain amplitude, loading rate, etc. [12]. Viscoelastic materials show evident hysteresis properties: stress trajectories are different in loading and unloading, which results in a hysteretic loop [13]. In other words, there is a certain phase difference between stress and strain, the stress–strain curve forms a loop marked as a hysteretic loop, and the area enclosed by hysteretic loop represents the loss of energy [14].

Studies on the hysteresis model of viscoelastic materials have attracted much attention with wide application of viscoelastic materials. Bouc–Wen model proposed by Bouc and further developed by Wen describes the hysteretic restoring force as a first-order differential equation, which has strong generality, high precision, and wide representation [15, 16]. Bingham model used by Stanway to describe the hysteresis effect of smart materials divides damping force into viscous damping force and Coulomb friction force, which promotes a theoretical study on the hysteresis properties of viscoelastic materials [17]. Chen et al. studied the hysteresis properties from the progress of resistor–capacitor (RC) charging and

discharging circuits. An RC operator was proposed to describe the hysteresis force of viscoelastic materials, which is excellent in terms of fitting and predictive power of the force–displacement properties of viscoelastic materials [18].

Based on above, a simplified tire physical model combined with the hysteresis properties of viscoelastic materials is proposed to explain the tire nonlinear dynamics in this study, and a tire model based on hysteresis property analysis (HysTire) under pure braking or cornering conditions is established. Specifically, the main contributions are as follows: (1) A simplified physical tire model that considers hysteresis of materials is established. In the model, tire is composed of a certain number of viscoelastic concave supports circling the rim, and a flexible high-friction crown belt in which elasticity and damping are ignored. When the crown belt is subjected to ground forces, the viscoelastic concave supports are compressed, and a tire force is generated. (2) The nonlinear dynamics of elastic hysteresis system are analyzed in-depth, and combined with RC operator, force–deformation property models of elastic hysteresis system are established in loading and unloading processes, respectively. (3) The force–deformation model of elastic hysteresis system was extended and applied to the tire nonlinear dynamics under pure braking or cornering conditions. A semi-empirical tire model based on hysteresis properties, HysTire, is established. HysTire is a unified expression tire model under pure braking or cornering conditions in the SAE tire coordinate system.

2 Physical model simplification of tires

In contrast to previous tire physical models, crown deformation has been emphasized [19, 20]. In this study, the tire body's deformation is considered as the main factor generating tire force. A physical tire model, as shown in Fig. 1a, named the concave support tire model, is established. As shown in Fig. 1a, a tire is considered to be composed of a certain number of viscoelastic concave supports circling the rim as tire body and a high-friction flexible belt of viscoelastic material as the tire crown. The elasticity and damping of tire body and crown are added as the tire's elasticity and damping. The angle that a concave ring is deflected relative to the rim by a longitudinal force in deformation area is written as ϕ_i. The deformation of a tire is the sum of the angles of all deflected concave rings, which is defined as the tire deformation angle ϕ, ϕ can be calculated as:

$$\phi = \phi_1 + \phi_2 + \phi_3 + \cdots + \phi_i + \cdots + \phi_j \tag{1}$$

where j is the number of deformed concave rings. When the crown belt is subjected to ground forces, the viscoelastic concave supports are compressed, and a tire force is generated. Figure 1b shows the tire deformation schematic of the established tire model under pure braking conditions. The friction force between crown and ground compresses the concave supports, which causes longitudinal deformation.

Deformation is the angle of tire-ground contact point relative to the wheel rim deflection, and the tire force is the composite force of all concave supports longitudinal elasticity force, damping force, and

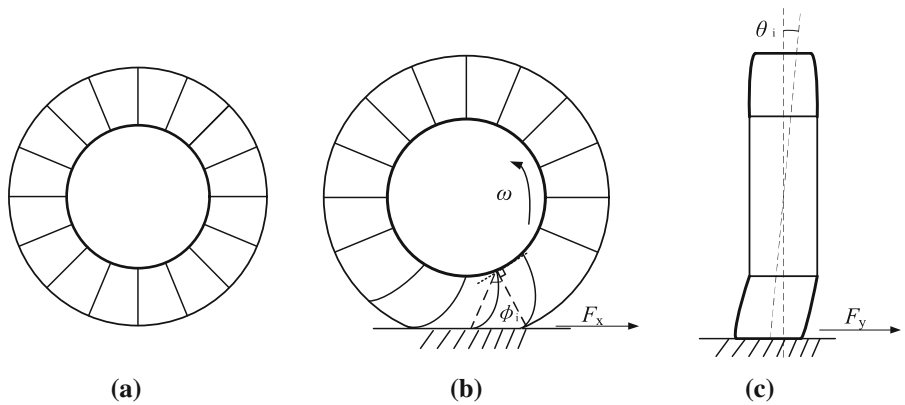

Fig. 1 Concave supports tire model: **a** schematic, **b** tire deformation under pure braking condition, and **c** tire deformation under pure cornering condition

hysteresis force. Figure 1c shows the tire deformation schematic of the established tire model under pure cornering conditions. The friction force between crown and ground compresses the concave supports, which causes lateral deformation. According to Fig. 1c, when the tire is stationary, deformation is the sum of distances between the deformed concaves contact patch center and the wheel plane. When the tire rolls, the deformation angle between the contact patch center of a concave support ring and the wheel plane is written as θ_i, and the tire lateral deformation angle θ is defined as the sum of angles caused by the deformed concave support rings. θ can be calculated as:

$$\theta = \theta_1 + \theta_2 + \theta_3 + \cdots + \theta_i + \cdots + \theta_q \tag{2}$$

where q is the number of deformed concave rings. The tire force is comprised of lateral elasticity force, damping force, and hysteresis force. The concave support tire model simplifies the tire into an elastic hysteresis system in all directions, which has at least three advantages: (1) The concave support tire model can qualitatively explain the generation and action mechanism of tire force and torque; (2) different with the crown friction model, the influence of structure (like aspect ratio, etc.) on tire performance is emphasized, which can provide a theoretical basis for tire structure design; (3) combining with the concave support tire model, the research achievements and methods of viscoelastic materials can be introduced in tire performance in the future.

3 Tire modeling under pure braking or cornering condition

3.1 Elastic hysteresis system model

The restoring force of viscoelastic materials is not only affected by the current amount of deformation but also by the deformation and velocity of the previous time. In other words, viscoelastic materials have a strong memory feature, showing that loading curve is inconsistent with the unloading curve. Figure 2 shows the force–displacement relationship of viscoelastic materials in loading and unloading processes, and the area enclosed by curve in the process of loading and unloading represents the loss of energy.

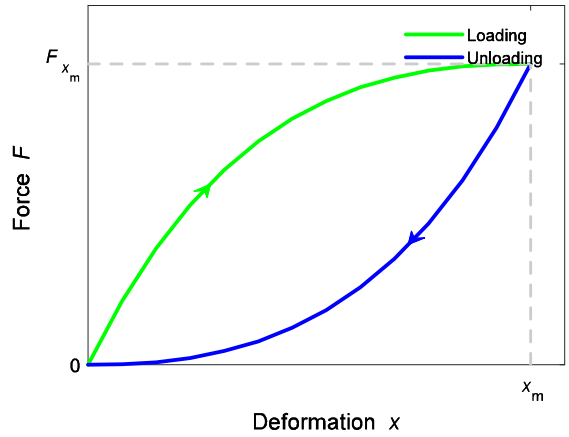

Fig. 2 Force–deformation relationship of viscoelastic materials in loading and unloading process

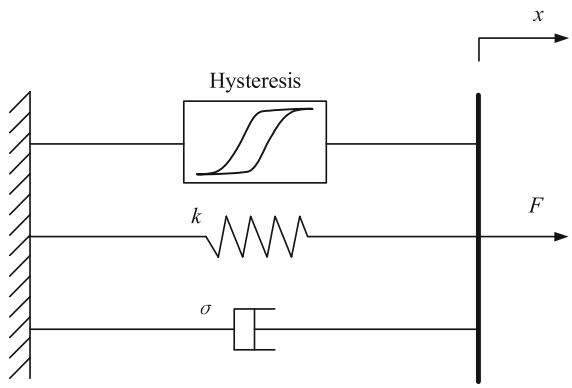

Fig. 3 Model of elastic hysteresis system for viscoelastic material

Generally, viscoelastic materials are simplified to the elastic hysteresis system model [21, 22], as shown in Fig. 3. The composite force F of the elastic hysteresis system mainly includes three parts: elasticity force (kx, N), damping force ($\sigma\dot{x}$, N), and hysteresis force (τz, N):

$$F(t) = kx(t) + \sigma\dot{x}(t) + \tau z(t) \tag{3}$$

where $x(t)$ is the deformation function, $\dot{x}(t)$ is the deformation speed, k is the elasticity coefficient, σ is the damping coefficient describing viscosity properties, τ is the hysteresis coefficient, and $z(t)$ is the hysteresis output.

The hysteresis operator $z(t)$ proposed by Chen et al. [20] named RC operator is expressed as:

$$z(t) = 1 - 2e^{-\frac{g_1(S)}{a}}, \text{ when } \dot{x}(t) > 0 \tag{4}$$

$$z(t) = -1 + 2e^{\frac{g_2(S)}{a}}, \text{when} \dot{x}(t) < 0 \tag{5}$$

$$\dot{z}(t) = 0, \text{ when } \dot{x}(t) = 0 \tag{6}$$

$$S_0 = {g_1}^{-1}\left(-\ln(\frac{(1 - z(t^*))}{2})a\right), x_0 = x(t^*), \text{ when change to load} \tag{7}$$

$$S_0 = {g_2}^{-1}\left(\ln\left(\frac{(1 + z(t^*))}{2}\right)a\right), x_0 = x(t^*), \text{ when change to unload} \tag{8}$$

$$S(t) = S_0 + x(t) - x_0 \tag{9}$$

where g_1 and g_2 are the monotonically increasing functions and satisfy $g_1(0_+) = g_2(0_-) = 0$, a is the hysteresis factor of the RC operator, S is an added virtual displacement variable at the new monotone excitation start time t^*, S_0 is the virtual displacement reference point, and x_0 is the displacement reference point.

When $\dot{x}(t) > 0$, $x = x_+$, and when $\dot{x}(t) < 0$, $x = x_-$, and the g_1 and g_2 in the RC operator are simplified into linear function, the force–displacement properties of the elastic hysteresis system can be summarized as:

$$F(x) = \begin{cases} kx_+ + \sigma\dot{x}_+ + \tau\left(1 - 2e^{-\frac{x}{a}}\right), & \dot{x} > 0 \\ kx_- + \sigma\dot{x}_- + \tau\left(-1 + 2e^{\frac{x}{a}}\right), & \dot{x} < 0 \\ F(x_m), \dot{x}(t) & = 0 \end{cases} \tag{10}$$

3.2 Longitudinal tire modeling under the pure braking condition

Based on the concave supports tire model, the mechanical properties of a tire under pure braking conditions are analyzed. The deflection angle of the tire crown relative to the rim is defined as the tire longitudinal deformation angle ϕ in Fig. 1. Figure 4 shows the relationship between tire longitudinal forces F_x and ϕ in process of tire braking from free rotation to completely locked. The process can be divided into three stages: loading stage I, loading stage II, and unloading stage. In the loading stage, when tire braking force applied by ground increases, the tire deformation angle ϕ gradually increases, and the tire crown can remain stationary with ground. Loading stage I overs when the static friction force between tire

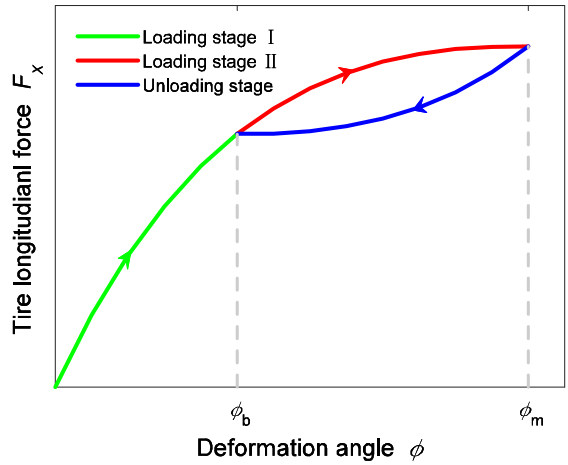

Fig. 4 Longitudinal force and deformation under pure braking condition

crown and ground reaches μF_N, the tire deformation angle is ϕ_b, where μ is the friction coefficient of road surface, and F_N is the vertical load of tire. At loading stage II, owing to the viscoelastic contact and adhesion between tire crown surface and road surface, the tire force continues to increase. The tire deformation angle ϕ further increases until the maximum deformation angle ϕ_m is reached, and the maximum static friction force between crown and ground is reached. As the sliding component of crown and ground increases, the friction between crown and ground transitions from static friction to sliding friction and cannot maintain the tire body deformation. Until the tire is locked, the friction turns into pure sliding friction, and the friction force stabilizes to μF_N. The tire deformation angle ϕ gradually decreases from the maximum deformation angle ϕ_m and stabilizes to ϕ_b. Loading stage II and unloading stage can be regarded as the elastic hysteresis system loading and unloading curves under the same deformation range, and the enclosed area represents the loss of energy.

In practical working conditions, it is difficult to measure the deformation angle ϕ of the tire, and the slip ratio is usually used to represent the wheel sliding component. There is a corresponding relationship between slip ratio and tire deformation angle. Figure 5 shows the relationship between tire force F_x and slip ratio s under pure braking conditions. The process of slip ratio from 0 to 1 shows the change process of tire from free rotation to completely locked. The longitudinal spring of the corresponding simplified tire model

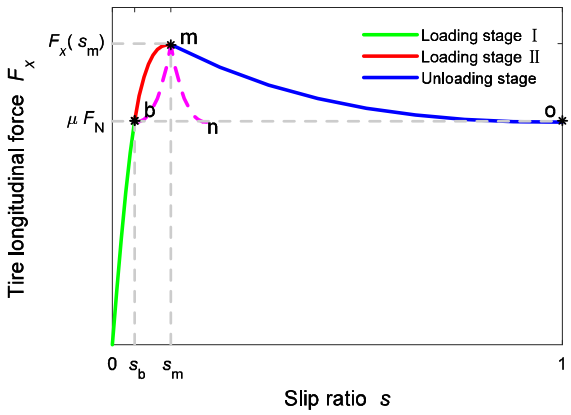

Fig. 5 Longitudinal force under pure braking condition

is compressed from 0 to ϕ_m, and bounce back to ϕ_b eventually. The relationship between tire force and slip ratio is divided into three stages: loading stage I, loading stage II, and the unloading stage. The slip ratio is calculated as the ratio of difference between vehicle speed and wheel speed and the vehicle speed, which is the speed difference between rim and tire crown. In loading stages I and II, the speed difference comes from the longitudinal compression of tire body, the tire crown and ground can still maintain no evident opposite slip. Slip ratio reaches to s_b from 0, and until the end of loading stage II, slip ratio reaches the optimal slip ratio s_m and the tire force reaches the maximum value F_{s_m}.

In unloading stage, the sliding component between crown and ground gradually increases, the slip ratio also increases, and the tire force starts to decrease. At the end of unloading stage, the slip ratio reaches 1, which means the tire-ground friction turns into pure sliding friction, and the tire force gradually decreases from the maximum value F_{s_m} to μF_N gradually. The tire force unloading process is shown in Fig. 4. From the analysis above, in Fig. 5, it can be seen that "mn" and "mo" are the unloading curves of one longitudinal deformation angle at the same time in different coordinates. It can be inferred that there is a corresponding relationship between $F_x - \phi$ and $F_x - s$ curves.

Since the specific relation between slip rate s and tire deformation angle ϕ is not known, the semi-empirical method is taken to identify the parameters in $F_x - s$. The change of slip ratio in steady-state tests is nearly linear, $\dot{s}$ can be taken as a constant. It is assumed that the optimal slip ratio s_m, the corresponding tire force F_{s_m}, road adhesion coefficient μ, and the tire vertical load F_N are known. In loading stage, the relationship between longitudinal tire force F_x and slip ratio s can be expressed as:

$$F_x(s) = \begin{cases} p_+ s + q_+ + r_+\left(1 - 2e^{-\frac{s}{w_+}}\right), & s < s_m \\ p_- s + q_- + r_-\left(-1 + 2e^{\frac{s}{w_-}}\right), & s > s_m \\ F_{s_m}, & s = s_m \end{cases} \tag{11}$$

where p_+, q_+, r_+, w_+, p_-, q_-, r_- and w_- are the parameters to be identified. To reduce the number of identification parameters and decrease the difficulty of identifying, the tire force during loading and unloading progress is assumed to be fully symmetry. As shown in Fig. 5, "bm" and "mb" are central symmetry about the point $(\frac{s_b+s_m}{2}, \frac{\mu F_N+F_m}{2})$, then the "mo" segment can be obtained by rotation, symmetry, and magnification of "bm". The corresponding unloading stage also can be expressed as:

$$\begin{aligned} F_x(s) = {} & F_{s_m} + \mu F_N - p_+(s_b + f_s(s - s_m)) \\ & - q_+ - r_+\left(1 - 2e^{-\frac{s_b + f_s(s-s_m)}{w_+}}\right), \text{ when } s > s_m \end{aligned} \tag{12}$$

$$F_x(s_b) = \mu F_N = p_+ s_b + q_+ + r_+(1 - 2e^{-\frac{s_b}{w_+}}) \tag{13}$$

$$f_s = \frac{s_m - s_b}{1 - s_m} \tag{14}$$

So the relationship between the longitudinal tire force F_x and slip ratio s also can be summarized as:

$$\begin{aligned} & F_x(s) = ps + q + r\left(1 - 2e^{-\frac{s}{w}}\right), \text{ when } s < s_m \\ & F_x(s) = F_{s_m} + \mu F_N - p(s_b + f_s(s - s_m)) \end{aligned} \tag{15}$$

$$-q - r\left(1 - 2e^{-\frac{s_b + f_s(s - s_m)}{w}}\right), \text{when} s > s_m \tag{16}$$

$$F_x(s) = F_{s_m}, \text{when} s = s_m \tag{17}$$

$$F_x(s_b) = \mu F_N = p s_b + q + r(1 - 2e^{-\frac{s_b}{w}}) \tag{18}$$

$$f_s = \frac{s_m - s_b}{1 - s_m} \tag{19}$$

where p, q, r and w are the parameters to be identified.

3.3 Lateral tire modeling under pure cornering condition

Similar to the variation process of tire longitudinal force, the lateral deformation angle θ of the tire is also difficult to measure in the practical application of tire, there is a correspondence between lateral deformation angle θ and slip angle α. And the lateral force also reaches the maximum value at a specific slip angle and then declines [23]. The same method is used to analyze lateral nonlinear dynamics of tires. Figure 6 shows the relationship between lateral force F_y and slip angle α. The change in the slip angle from 0° to 90° corresponds to spring lateral compression and partial rebound of the simplified tire model. The lateral force under pure cornering condition in Fig. 6 can still be divided into three stages: loading stage I, loading stage II, and unloading stage. In loading stages I and II, until the end of loading stage II, the slip angle reaches to α_{m} and the tire lateral force reaches the maximum value $F_{\alpha_{\mathrm{m}}}$. There is no evident opposite slip between tire crown and ground during the processes. In unloading stage, the slip angle exceeds α_{m} until it reaches 90°, the lateral tire force decreases gradually from the maximum value $F_{\alpha_{\mathrm{m}}}$ to μF_{N}, and μF_{N} is the pure sliding friction force.

It is assumed that the maximum tire lateral force $F_{\alpha_{\mathrm{m}}}$, corresponding slip angle α_{m}, road adhesion coefficient μ, and the tire vertical load F_{N} are known. In loading stage, the relationship between tire lateral force F_y and slip angle α can be expressed as:

$$F_{\mathrm{y}}(\alpha) = p\alpha + q + r\left(1 - 2\mathrm{e}^{-\frac{\alpha}{w}}\right), \text{ when } \alpha < \alpha_{\mathrm{m}} \tag{20}$$

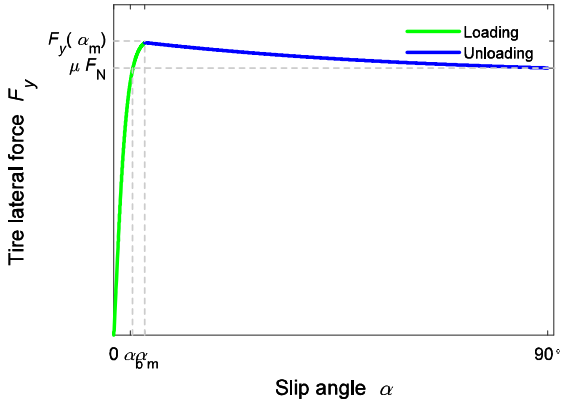

Fig. 6 Lateral force under pure cornering condition

where p, q, β and r are the parameters to be identified.

The corresponding unloading stage can be expressed as:

$$F_{\mathrm{y}}(\alpha) = F_{\alpha_m} + \mu F_{\mathrm{N}} - p(\alpha_b + f_\alpha(\alpha - \alpha_m)) - q - r\left(1 - 2e^{-\frac{\alpha_{\mathrm{b}} + f_\alpha(\alpha - \alpha_m)}{w}}\right), \text{ when } \alpha > \alpha_m \tag{21}$$

$$F_{\mathrm{y}}(\alpha) = F_{\alpha_{\mathrm{m}}}, \text{when } \alpha = \alpha_{\mathrm{m}} \tag{22}$$

$$F_{\mathrm{y}}(\alpha_{\mathrm{b}}) = \mu F_{\mathrm{N}} = p\alpha_{\mathrm{b}} + q + r(1 - 2\mathrm{e}^{-\frac{\alpha_{\mathrm{b}}}{w}}) \tag{23}$$

$$f_\alpha = \frac{\alpha_{\mathrm{m}} - \alpha_{\mathrm{b}}}{90 - \alpha_{\mathrm{m}}} \tag{24}$$

3.4 Tire aligning torque modeling

The alignment torque M_Z is torque around tire OZ axis and is generated under cornering conditions. This quantity can be expressed numerically as

$$M_Z = F_y \cdot d \tag{25}$$

where d is the offset distance between the origin of F_{y} and tire geometric center point, which is marked as the pneumatic trail. The pneumatic trail under pure cornering condition shown in Fig. 7 can be expressed as

$$d = p_{\mathrm{d}}\mathrm{e}^{-\frac{\alpha}{q_{\mathrm{d}}}} - 2r_{\mathrm{d}}\mathrm{e}^{-\frac{\alpha}{w_{\mathrm{d}}}} \tag{26}$$

Synthesizing Eqs. (15)–(24), the HysTire under pure braking or cornering conditions is proposed. Specifically:

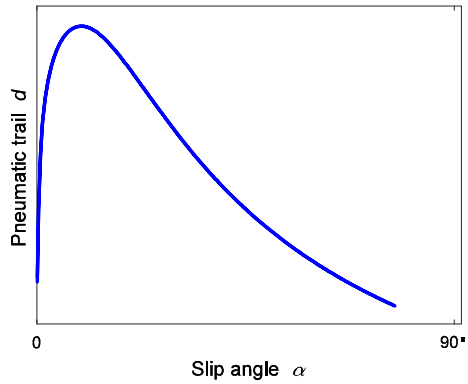

Fig. 7 Pneumatic trail under pure cornering condition

$$\begin{aligned} F(x) &= px + q + r\left(1 - 2e^{-\frac{x}{w}}\right), \text{ when } x < x_{\mathrm{m}} \\ F(x) &= F_{x_{\mathrm{m}}} + \mu F_{\mathrm{N}} - p(x_{\mathrm{b}} + f_{\mathrm{x}}(x - x_{\mathrm{m}})) \end{aligned} \tag{27}$$

$$-q - r\left(1 - 2e^{-\frac{x_{\mathrm{b}} + F_{\mathrm{x}}(x - x_{\mathrm{m}})}{w}}\right), \text{ when } x > x_{\mathrm{m}} \tag{28}$$

$$F(x) = F_{x_{\mathrm{m}}}, \text{when } x = x_{\mathrm{m}} \tag{29}$$

$$M_z = F(\alpha) \cdot d \tag{30}$$

$$d = p_{\mathrm{d}} e^{-\frac{\alpha}{q_{\mathrm{d}}}} - 2r_{\mathrm{d}} e^{-\frac{\alpha}{w_{\mathrm{d}}}} \tag{31}$$

$$F_{x_{\mathrm{b}}} = \mu F_N = p x_{\mathrm{b}} + q + r\left(1 - 2e^{-\frac{x_{\mathrm{b}}}{w}}\right) \tag{32}$$

$$F_{\mathrm{x}} = \frac{x_{\mathrm{m}} - x_{\mathrm{b}}}{x_{\mathrm{o}} - x_{\mathrm{m}}} \tag{33}$$

where $F(x)$ is the tire's longitudinal force or lateral force at the SAE coordinate, the corresponding independent variable x is the tire slip ratio s or slip angle α; x_{b}, x_{m} and x_{o} represent the starting point of loading, the maximum point, and the end point of unloading, respectively, where $s_{\mathrm{o}} = 1$, $\alpha_{\mathrm{o}} = 90^{\circ}$ and the tire forces at the starting point of loading are equal to the endpoint of unloading, which equal to the pure sliding friction force μF_{N}; f is the zoom factor; p, q, r, w, p_{d},q_{d}, r_{d}, and w_{d} are the parameters to be identified.

4 Parameter identification

Based on the proposed HysTire in Sect. 3, the parameters in models are identified using test data of the pure braking condition and pure cornering condition. A genetic algorithm is used to identify the parameters of HysTire. The initial population size of the genetic algorithm is 20; the selection algorithm adopts a random distribution selection algorithm; the crossover method is scattered crossover, the crossover probability is 0.8, and the mutation probability is 0.2. Gaussian function method is used for mutation, and random numbers with Gaussian distribution and mean 0 are generated and added to the parent generation, the scale is 0.5 and the compression is 0.7. As shown in Fig. 8, the specific identification process under two pure conditions is presented. The identification process of HysTire under pure braking conditions is shown in Fig. 8a. When $\dot{F}(s) > 0$, the longitudinal force increases with slip ratio. Until $\dot{F}(s) = 0$, the longitudinal force reaches its maximum, and the slip ratio at this point is s_{m}, which is marked as the maximum point. At $0 - s_{\mathrm{m}}$ stage. The longitudinal model at $0 - s_{\mathrm{m}}$ stage can be obtained by obtaining the parameters p, q, r, and w. When $\dot{F}(s) < 0$, the slip ratio ranges from s_{m} to the maximum slip ratio $s_{\mathrm{o}} = 1$. s_{o} is marked as the end point of unloading, and the corresponding tire force $F_{s_{\mathrm{o}}}$ satisfy $F_{s_{\mathrm{o}}} = \mu F_{\mathrm{N}}$. A point marked s_{b} is the start point of loading stage II at $0 - s_{\mathrm{m}}$ stage, whose corresponding tire force $F_{s_{\mathrm{b}}}$ satisfies $F_{s_{\mathrm{b}}} = F_{s_{\mathrm{o}}} = \mu F_{\mathrm{N}}$. And s_{b} can be obtained by the inverse solution of HysTire longitudinal model at $0 - s_{\mathrm{m}}$ stage. Thus far, the tire's HysTire longitudinal model can be obtained by taking all the parameters p, q, r, w, s_{b}, s_{m},s_{o}, $F_{s_{\mathrm{m}}}$, and μF_{N} into the HysTire.

The identification process of HysTire under pure cornering conditions is shown in Fig. 8b. When $\dot{F}(\alpha) > 0$, the lateral force increases with slip angle. Until $\dot{F}(\alpha) = 0$, the lateral force reaches its maximum, and the slip angle at this point is α_{m}, which is marked as the maximum point. At $0 - \alpha_{\mathrm{m}}$ stage. The lateral model at $0 - \alpha_{\mathrm{m}}$ stage can be obtained by obtaining the parameters p, q, r, and w. When $\dot{F}(\alpha) < 0$, the slip angle ranges from α_{m} to the maximum slip angle $\alpha_{\mathrm{o}} = 90^{\circ}$. α_{o} is marked as the end point of unloading, and the corresponding tire lateral force $F_{\alpha_{\mathrm{o}}}$ satisfies $F_{\alpha_{\mathrm{o}}} = \mu F_{\mathrm{N}}$. A point marked α_{b} is the start point of loading II at $0 - \alpha_{\mathrm{m}}$ stage, whose corresponding tire lateral force $F_{\alpha_{\mathrm{b}}}$ satisfies $F_{\alpha_{\mathrm{b}}} = F_{\alpha_{\mathrm{o}}} = \mu F_{\mathrm{N}}$. In addition, α_{b} can be obtained by the inverse solution of HysTire lateral model at $0 - \alpha_{\mathrm{m}}$ stage. Thus far, the lateral tire model can be obtained by taking all the parameters p, q, r, w, α_{b}, α_{m}, α_{o}, $F_{\alpha_{\mathrm{m}}}$ and μF_{N} into the HysTire. Because the tire lateral model is known, the aligning torque model can be obtained by identifying the pneumatic trail d. The aligning torque model can be obtained by obtaining the parameters p_{d}, q_{d}, r_{d} and w_{d}.

Through the identification process of tire nonlinear dynamics, it can be seen that the HysTire requires fewer test data compared with the MF, which means lower test and time costs. As a result, HysTire have great value in engineering applications.

5 Results and discussion

To verify the effectiveness of HysTire, the steady-state tests of two Hoosier tires (type: 18.0/7.5–10 R25B and

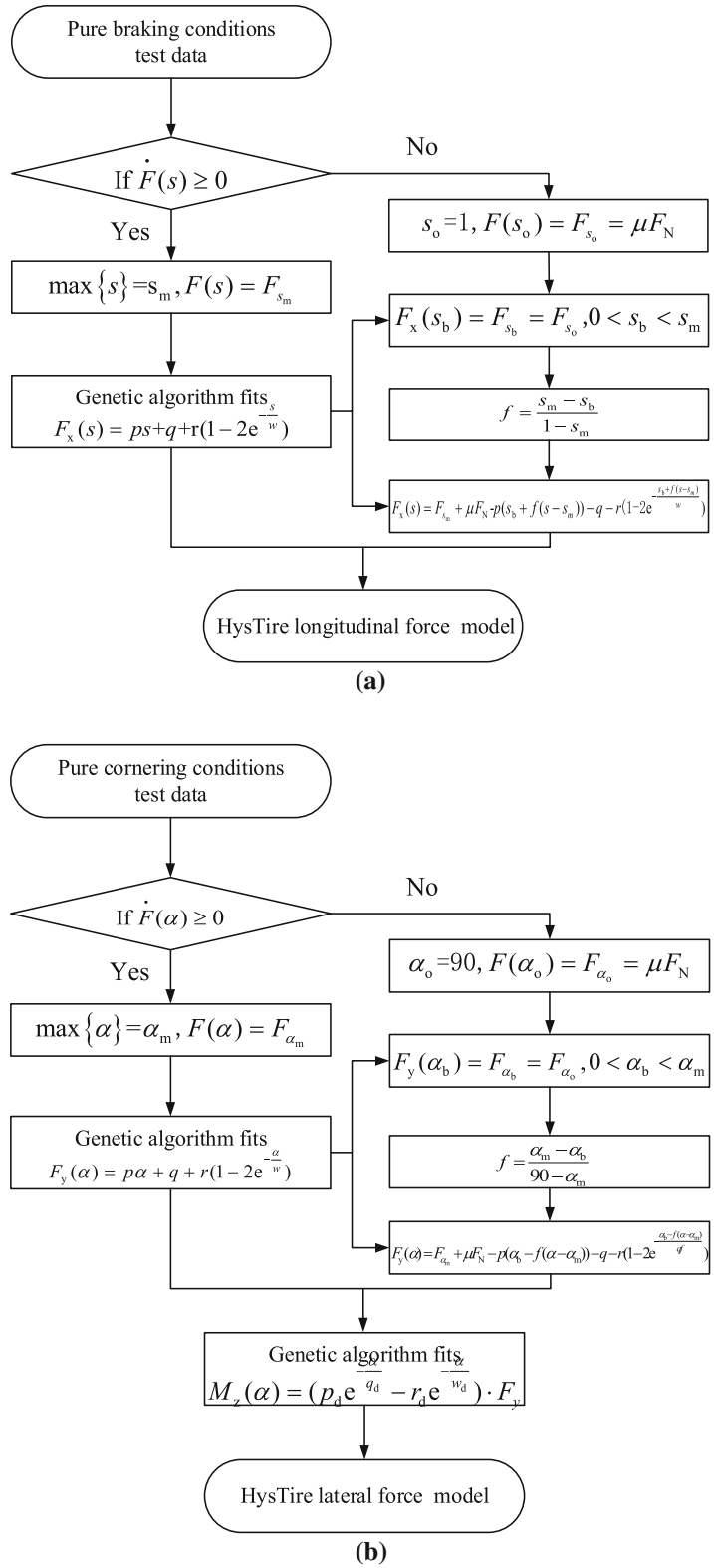

Fig. 8 HysTire parameter identification processes: **a** pure braking condition and **b** pure cornering condition

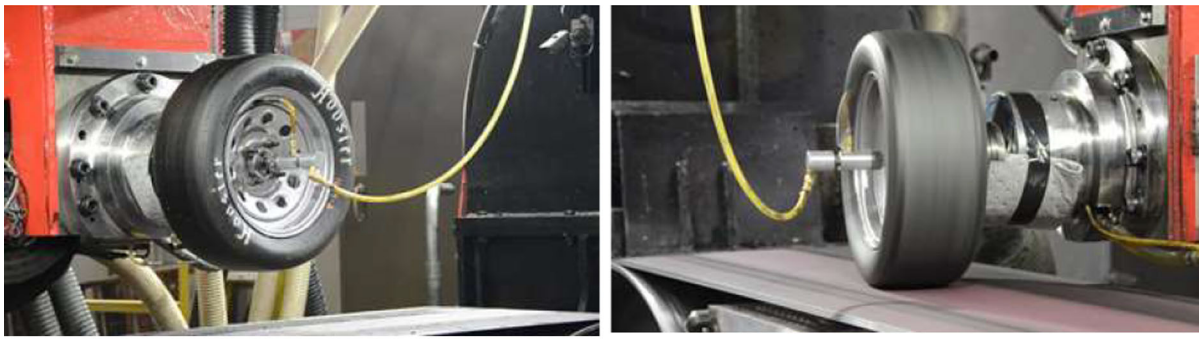

(a) (b)

Fig. 9 Tire test platform: **a** longitudinal force tests and **b** lateral force tests

20.5/6.0–13 R25B A2500) are carried out in the tire test platform, as shown in Fig. 9.

Test data of the two tires are fitted using MF and HysTire, and the model identification results are shown in Figs. 10 and 11. The MSE comparison between the two models' fitting results and test results of tires A and B is shown in Fig. 12. Low load, medium load, and heavy load conditions of one tire are represented from left to right. It can be seen that the MSE value of Hystire is very close to or even smaller than that of MF in each working condition. Both Hystire and MF present very high description accuracy for tire nonlinear dynamics in steady state. In addition, as shown in Fig. 11a, in the case of limited test data, the MF is poor in terms of predictive and extrapolative in undone test data. However, under the same test data, HysTire is not only good in terms of fitting the test data but also excellent in terms of predicting the mechanical behavior of tires. HysTire revealed the variation rules of tire nonlinear dynamics and established the internal relationship of tire nonlinear dynamics.

6 Conclusions

In this study, the tire nonlinear dynamics were explained in a new way which combined a simplified physical tire model and hysteresis properties. A semi-empirical tire model named HysTire was established, a unified expression tire model under pure braking or cornering conditions in the SAE tire coordinate system. Specifically, (1) a simplified physical tire model that considers hysteresis was proposed. In the model, a tire is considered to be composed of a certain number of viscoelastic concave supports circling the rim and a flexible high-friction crown belt in which elasticity and damping are ignored. When the crown belt is subjected to ground forces, the viscoelastic concave supports are compressed, and a tire force is generated. (2) The nonlinear dynamics of the elastic hysteresis system were analyzed deeply, and combined with the RC operator, force–deformation property models of the elastic hysteresis system were established in the loading and unloading processes. (3) The interaction between the tire and ground under pure braking or cornering conditions was also divided into loading and unloading processes, and the variation rule of tire nonlinear dynamics in the loading and unloading process was analyzed. The internal correlation between the tire nonlinear dynamics under small slip ratios or slip angles and large slip ratios or slip angles was revealed through the study of tire nonlinear dynamics in the loading and unloading process under pure braking or cornering conditions. Thus, a new theoretical explanation was proposed for tire nonlinear dynamics under pure braking or cornering conditions, and a new tire model, HysTire, was established.

7 Future perspectives

HysTire introduced the hysteresis theory into the tire nonlinear dynamics explanation, a new theoretical explanation of tire nonlinear dynamics, and has been proven to achieve high fitting accuracy. Therefore, HysTire is worth further improvement.

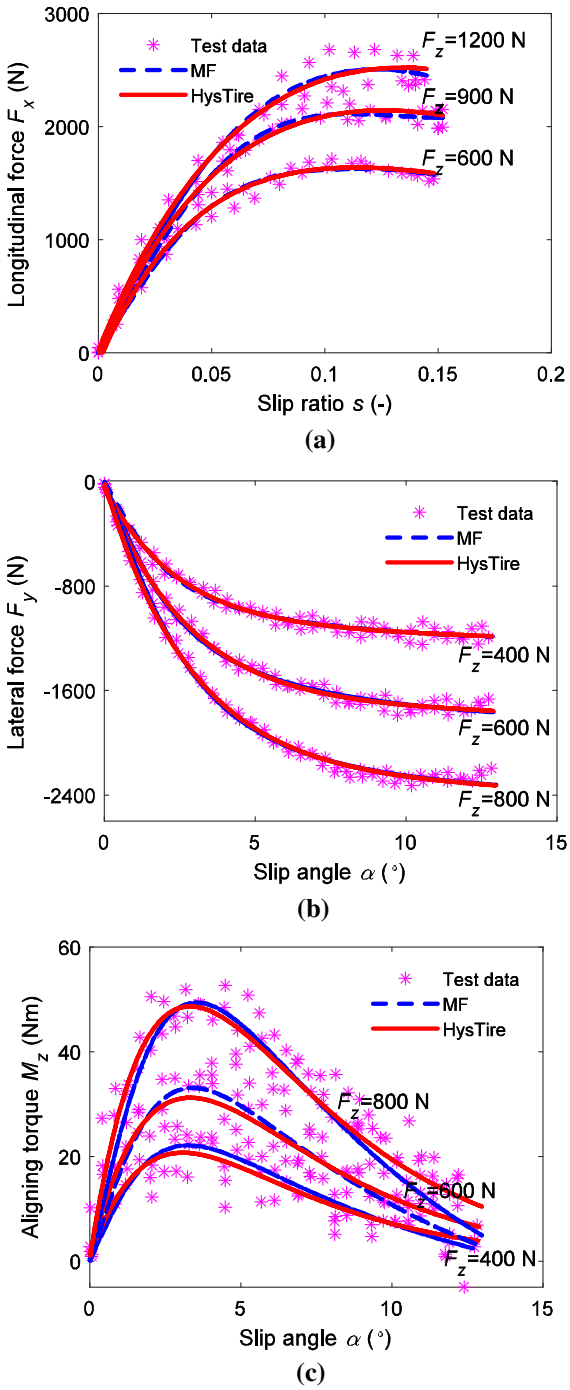

Fig. 10 Tire models and validating 18.0/7.5–10 R25B tire tests data: **a** longitudinal force, **b** lateral force, and **c** aligning torque

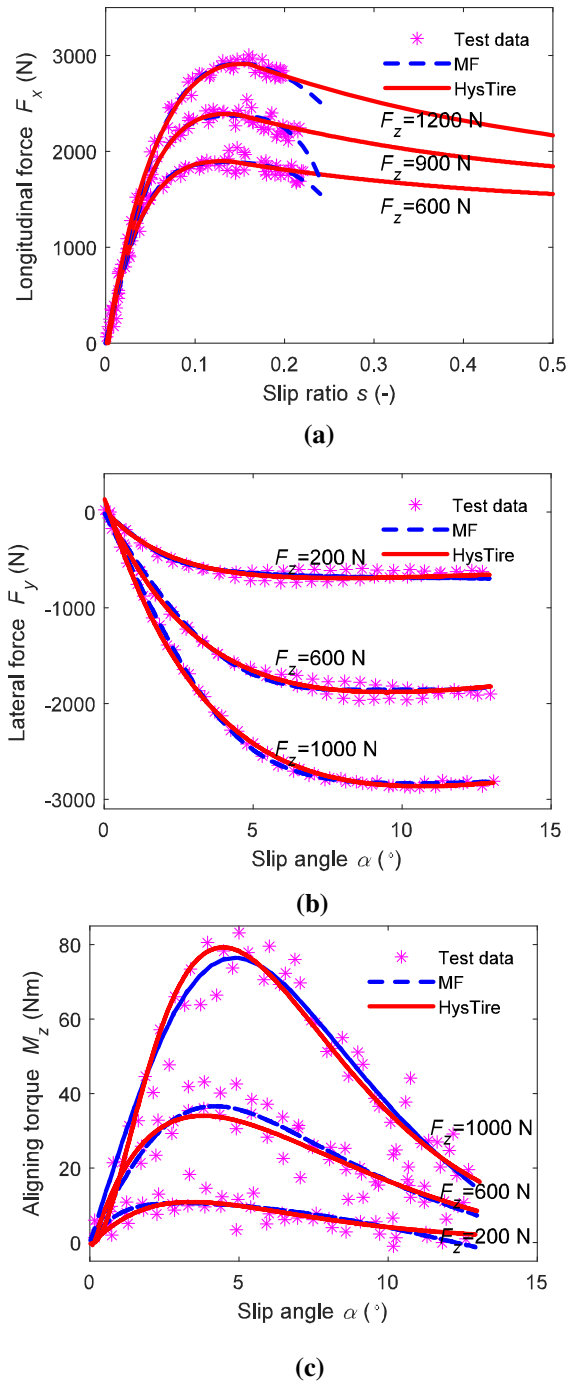

Fig. 11 Tire models and validating 20.5/6.0–13 R25B A2500 tire test data: **a** longitudinal force, **b** lateral force, and **c** aligning torque

(1) Based on the concave support tire model, the tire nonlinear dynamics under combined slip conditions should be studied, and the HysTire under combined slip conditions may be established.

(2) Based on the hysteresis properties, the effects of tire rotation speed or braking force loading speed on the nonlinear dynamics of tires should

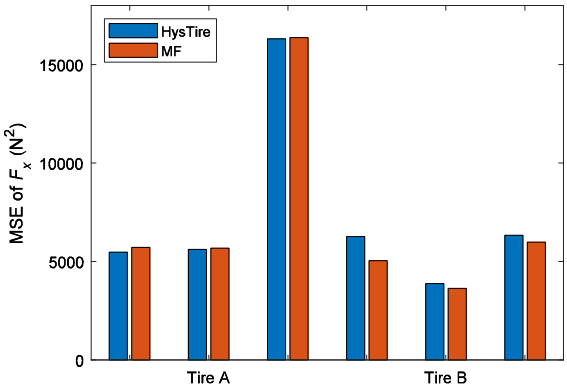

(a)

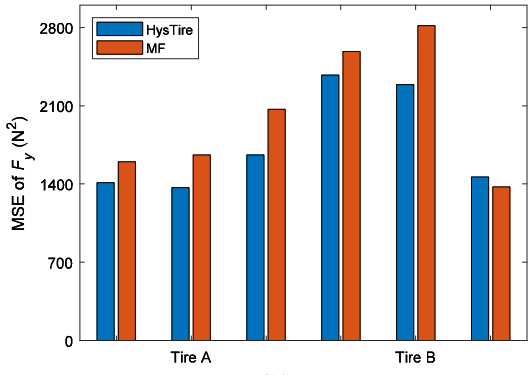

(b)

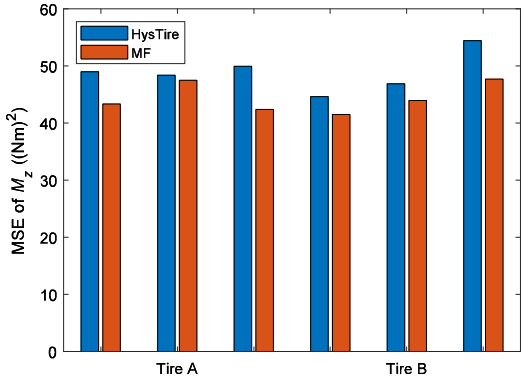

(c)

Fig. 12 The MSE comparison between the two models for tires A and B: **a** longitudinal force, **b** lateral force, and **c** aligning torque

be studied further, and the HysTire that introduces the "change ratio of slip ratio" may be established.

Funding This study is funded by the National Natural Science Foundation of China (Grant No. 52272392) and the Innovation Project of New Energy and Intelligent Connected Vehicle of Anhui Province.

Data availability The datasets generated during and/or analyzed during the current study are available from the corresponding author on reasonable request.

Declarations

Conflict of interest The authors declare no potential conflicts of interest for the research, authorship, and/or publication of this article.

References

1. Sun, X., Zhang, H., Cai, Y., Wang, S., Chen, L.: Hybrid modeling and predictive control of intelligent vehicle longitudinal velocity considering nonlinear tire dynamics. Nonlinear Dyn. **97**, 1051–1066 (2019)
2. Zhuang, Y., Song, Z., Gao, X., Yang, X., Liu, W.: A combined-slip physical tire model based on the vector distribution considering tire anisotropic stiffness. Nonlinear Dyn. **108**, 2961–2976 (2022). https://doi.org/10.1007/s11071-022-07462-y
3. Svendenius, J., Gäfvert, M., Bruzelius, F., Hultén, J.: Experimental validation of the brush tire model. Tire Sci. Technol. **37**, 122–137 (2009). https://doi.org/10.2346/1.3130985
4. Edwards, D.L., Bevly, D.M.: A method to estimate critical tire properties using nonlinear tire models. ASME Int. Mech. Eng. Congr. Expos. **43033**, 1137–1146 (2007)
5. Schmeitz, A.J.C., Besselink, I.J.M., Jansen, S.T.H.: TNO MF-SWIFT. Veh. Syst. Dyn. **45**, 121–137 (2007). https://doi.org/10.1080/00423110701725208
6. Gipser, M.: FTire: a physically based application-oriented tyre model for use with detailed MBS and finite-element suspension models. Veh. Syst. Dyn. **43**, 76–91 (2005). https://doi.org/10.1080/00423110500139940
7. Pacejka, H.B., Bakker, E.: The magic formula tyre model. Veh. Syst. Dyn. **21**, 1–18 (1992). https://doi.org/10.1080/00423119208969994
8. Mi, T., Stépán, G., Takacs, D., Chen, N.: Vehicle shimmy modeling with Pacejka's magic formula and the delayed tire model. J. Comput. Nonlinear Dyn. (2020). https://doi.org/10.1115/1.4045943
9. Guo, K.H., Lu, D., Chen, S.K., Lin, W.C., Lu, X.P.: The UniTire model: a nonlinear and non-steady-state tyre model for vehicle dynamics simulation. Veh. Syst. Dyn. **43**, 341–358 (2005). https://doi.org/10.1080/00423110500140690
10. Guo, K.: UniTire: unified tire model. JME **52**, 90 (2016). https://doi.org/10.3901/JME.2016.12.090
11. Bhave, T., Tehrani, M., Ali, M., Sarvestani, A.: Hysteresis friction and nonlinear viscoelasticity of rubber composites. Compos. Commun. **9**, 92–97 (2018). https://doi.org/10.1016/j.coco.2018.07.001

12. Younesian, D., Hosseinkhani, A., Askari, H., Esmailzadeh, E.: Elastic and viscoelastic foundations: a review on linear and nonlinear vibration modeling and applications. Nonlinear Dyn. **97**, 853–895 (2019). https://doi.org/10.1007/s-11071-019-04977-9
13. Knauss, W.G.: A review of fracture in viscoelastic materials. Int J Fract. **196**, 99–146 (2015). https://doi.org/10.1007/s10704-015-0058-6
14. Carboni, B., Lacarbonara, W.: Nonlinear dynamic characterization of a new hysteretic device: experiments and computations. Nonlinear Dyn. **83**, 23–39 (2016). https://doi.org/10.1007/s11071-015-2305-9
15. Vaiana, N., Sessa, S., Rosati, L.: A generalized class of uniaxial rate-independent models for simulating asymmetric mechanical hysteresis phenomena. Mech. Syst. Signal Process. **146**, 106984 (2021). https://doi.org/10.1016/j.ymssp.2020.106984
16. Bouc, R.: A mathematical model for hysteresis. Acta Acust. Acust. **24**, 16–25 (1971)
17. Wen, Y.-K.: Method for random vibration of hysteretic systems. J .Eng. Mech. Div. **102**, 249–263 (1976)
18. Atkinson, C., El-Ali, K.: Some boundary value problems for the Bingham model. J. Non-Newton. Fluid Mech. **41**, 339–363 (1992). https://doi.org/10.1016/0377-0257(92)87006-W
19. Chen, P., Bai, X.-X., Qian, L.-J., Choi, S.-B.: An approach for hysteresis modeling based on shape function and memory mechanism. IEEE/ASME Trans. Mechatron. **23**, 1270–1278 (2018). https://doi.org/10.1109/TMECH.201-8.28334-59
20. Lu, Y., Zhang, J., Yang, S.: Study on improvement of LuGre dynamical model and its application in vehicle handling dynamics. J Mech Sci Technol **33**, 545–558 (2019). https://doi.org/10.1007/s12206-019-0108-5
21. Kobayashi, T., Katsuyama, E., Sugiura, H., Hattori, Y., Ono, E., Yamamoto, M.: Theoretical analysis of tyre slip power dissipation mechanism using brush model. Veh. Syst. Dyn. **58**, 1242–1256 (2020). https://doi.org/10.1080/00423114.2019.1612926
22. Yun, K.S., Youn, S.K.: Microstructural topology optimization of viscoelastic materials of damped structures subjected to dynamic loads. Int. J. Solids Struct. **147**, 67–79 (2018). https://doi.org/10.1007/s00158-015-1305-1
23. Penas, R., Balmes, E., Gaudin, A.: A unified non-linear system model view of hyperelasticity, viscoelasticity and hysteresis exhibited by rubber. Mech. Syst. Signal Process. **170**, 108793 (2022). https://doi.org/10.1016/j.y-mssp.2021.108793
24. Vorotovic, G.S., Rakicevic, B.B., Mitic, S.R., Stamenkovic, D.D.: Determination of cornering stiffness through integration of a mathematical model and real vehicle exploitation parameters. FME Trans. **41**, 66–71 (2013)